A Section 508–conformant HTML version of this article is available at https://doi.org/10.1289/EHP7679.

Assessing the Distribution of Air Pollution Health Risks within Cities: A Neighborhood-Scale Analysis Leveraging High-Resolution Data Sets in the Bay Area, California

Veronica A. Southerland,[1] Susan C. Anenberg,[1] Maria Harris,[2] Joshua Apte,[3] Perry Hystad,[4] Aaron van Donkelaar,[5,6] Randall V. Martin,[6] Matt Beyers,[7] and Ananya Roy[2]

[1]Milken Institute School of Public Health, George Washington University, Washington, District of Columbia, USA
[2]Environmental Defense Fund, San Francisco, California, USA
[3]Department of Civil & Environmental Engineering and School of Public Health, University of California, Berkeley, USA
[4]School of Biological and Population Health Sciences, College of Public Health and Human Sciences, Oregon State University, Corvallis, Oregon, USA
[5]Department of Physics and Atmospheric Science, Dalhousie University, Halifax, Nova Scotia, Canada
[6]Energy, Environmental & Chemical Engineering, McKelvey School of Engineering, Washington University in St. Louis, St. Louis, Missouri, USA
[7]Alameda County Public Health Department, Oakland, California, USA

Background: Air pollution-attributable disease burdens reported at global, country, state, or county levels mask potential smaller-scale geographic heterogeneity driven by variation in pollution levels and disease rates. Capturing within-city variation in air pollution health impacts is now possible with high-resolution pollutant concentrations.

Objectives: We quantified neighborhood-level variation in air pollution health risks, comparing results from highly spatially resolved pollutant and disease rate data sets available for the Bay Area, California.

Methods: We estimated mortality and morbidity attributable to nitrogen dioxide (NO_2), black carbon (BC), and fine particulate matter [PM $\leq$2.5 μm in aerodynamic diameter ($PM_{2.5}$)] using epidemiologically derived health impact functions. We compared geographic distributions of pollution-attributable risk estimates using concentrations from *a*) mobile monitoring of NO_2 and BC; and *b*) models predicting annual NO_2, BC and $PM_{2.5}$ concentrations from land-use variables and satellite observations. We also compared results using county vs. census block group (CBG) disease rates.

Results: Estimated pollution-attributable deaths per 100,000 people at the 100-m grid-cell level ranged across the Bay Area by a factor of 38, 4, and 5 for NO_2 [mean = 30 (95% CI: 9, 50)], BC [mean = 2 (95% CI: 1, 2)], and $PM_{2.5}$, [mean = 49 (95% CI: 33, 64)]. Applying concentrations from mobile monitoring and land-use regression (LUR) models in Oakland neighborhoods yielded similar spatial patterns of estimated grid-cell–level NO_2-attributable mortality rates. Mobile monitoring concentrations captured more heterogeneity [mobile monitoring mean = 64 (95% CI: 19, 107) deaths per 100,000 people; LUR mean = 101 (95% CI: 30, 167)]. Using CBG-level disease rates instead of county-level disease rates resulted in 15% larger attributable mortality rates for both NO_2 and $PM_{2.5}$, with more spatial heterogeneity at the grid-cell–level [NO_2 CBG mean = 41 deaths per 100,000 people (95% CI: 12, 68); NO_2 county mean = 38 (95% CI: 11, 64); $PM_{2.5}$ CBG mean = 59 (95% CI: 40, 77); and $PM_{2.5}$ county mean = 55 (95% CI: 37, 71)].

Discussion: Air pollutant-attributable health burdens varied substantially between neighborhoods, driven by spatial variation in pollutant concentrations and disease rates. https://doi.org/10.1289/EHP7679

Introduction

Air pollution is associated with a large burden of death and disability worldwide, with fine particulate matter [PM $\leq$2.5 μm in aerodynamic diameter ($PM_{2.5}$)] estimated to be responsible for 4.9 million deaths globally in 2015 (GBD 2017 Risk Factor Collaborators 2018). Nitrogen dioxide (NO_2), a traffic-related air pollutant, is also linked with adverse health outcomes, although it is often not quantified in pollution-attributable disease burden studies, potentially because coarsely resolved concentration estimates are often unable to capture highly spatially variable patterns in NO_2 (Anenberg et al. 2017). Recent advances in the understanding of the health effects of NO_2, meta-analyses (Atkinson and Butland 2018; U.S. EPA 2016), and published recommendations from a committee of scientists (Atkinson and Butland 2018) provide guidance on evaluating and interpreting NO_2, as a marker of the mixture of traffic air pollution, in health impact assessments.

Much of the air pollution disease burden is concentrated in cities (Anenberg et al. 2019). Cities are home to about half the world's population (United Nations 2019) and 80% of the U.S. population (U.S. Census Bureau 2018). Many cities also experience both high air pollution levels (Krzyzanowski et al. 2014; Marlier et al. 2016) and health inequity challenges (Grant et al. 2017; Kioumourtzoglou et al. 2015; Stephens 2018). However, estimated health impacts from air pollution have typically been reported at the country, state, or county level, masking potential heterogeneity in impacts at fine spatial scales.

Understanding how air pollution-related health risks vary within cities could help inform policies aimed at improving public health and reducing population disparities in exposure and risk in urban areas. Recent efforts have estimated air pollution health impacts at the city level, finding dramatic variation in health risks across cities globally (Achakulwisut et al. 2019; Anenberg et al. 2019). However, only a limited number of studies have assessed air pollution mortality risks at the neighborhood level, and these have focused on individual cities and have generally not compared the advantages and disadvantages of different concentration data sources (Brønnum-Hansen et al. 2018; Kheirbek et al. 2013; Kihal-Talantikite et al. 2018; Martenies et al. 2018; Mueller et al. 2017, 2018, 2020; Pierangeli et al. 2020). In addition, these previous city-scale studies may not have captured the spatial distribution of air pollution-related health risks given that the grid sizes used in those studies can dilute

Address correspondence to Susan C. Anenberg, Milken Institute School of Public Health, George Washington University, Washington, DC 20052 USA. Telephone: (202) 994-2392. Email: sanenberg@gwu.edu

Supplemental Material is available online (https://doi.org/10.1289/EHP7679).

The authors declare they have no actual or potential competing financial interests.

Received 15 June 2020; Revised 10 February 2021; Accepted 24 February 2021; Published 31 March 2021.

hotspots of high concentrations co-located with large populations (Fenech et al. 2018; Korhonen et al. 2019; Li et al. 2016; Punger and West 2013). Beyond horizontal grid size, the resolution of emissions inputs to estimate concentrations can also influence the resulting estimated air pollution-related health impacts. Two studies examining the impacts of both varying horizontal grid and emissions resolution on health burden estimates report mixed results. Paolella et al. (2018) reported a reduced ability of coarse resolution concentration estimates to identify disparities in health impacts, whereas a study by Thompson et al. (2014) found limited difference for $PM_{2.5}$ attributable health impacts with varying emissions and grid resolution (Thompson et al. 2014).

Despite these differences, finer-resolution exposure estimates may decrease the potential for exposure misclassification. Estimating air pollution health impacts at the "hyperlocal" scale (resolving neighborhoods within cities) is now possible with high-resolution pollutant concentrations derived from mobile monitoring and modeling, complemented by satellite remote sensing. Here, we exploit a novel and extremely high-spatial–resolution pollution concentration data set from mobile monitoring of NO_2 and black carbon (BC) using Google Street View (hereafter referred to as Street View) cars throughout the Bay Area, California, from 2015 to 2017. Previously, these measurements have been used to create street-level annual average concentrations of NO_2 and BC, a land-use regression (LUR) model (Messier et al. 2018), and an epidemiological analysis of relationships between long-term exposure to NO_2 and cardiovascular disease (CVD) outcomes (Alexeeff et al. 2018), all for Oakland, California. Jointly, these efforts demonstrated the application of highly resolved concentration data to analyze intra-urban variation in pollutant exposure and the associated health risks. Building upon these efforts, here we use Street View concentrations to assess air pollution health impacts at the neighborhood scale. To our knowledge, our analysis is the first to use air pollution levels from sensor-aided mobile monitoring in a health impact assessment. Given that most cities globally do not have the same availability of highly spatially resolved concentration data as the Bay Area, we compare pollutant-attributable health risks estimated using the Street View concentrations vs. less data- and resource-intensive predictive models. These predictive models use land-use variables and satellite observations of aerosol optical depth (AOD) that can be applied in any city globally to create street-level annual average concentrations of NO_2 and $PM_{2.5}$ (Larkin et al. 2017; van Donkelaar et al. 2016).

Neighborhood-level health risks from air pollution are driven not just by exposure levels but also by baseline disease rates, which themselves vary within cities (e.g., Fann et al. 2012), influencing attributable mortality estimates (Chowdhury and Dey 2016; Hubbell et al. 2009). Prior air pollution morbidity and mortality assessments have typically used baseline disease rates at the state, county, or national level owing to the limited availability of more highly resolved health data (Alotaibi et al. 2019; Caiazzo et al. 2013; Cohen et al. 2017; Fann et al. 2012, 2017; Zhang et al. 2018). Here, in addition to comparing across concentration data sets, we also assess the influence of baseline disease rates with varying spatial resolutions (i.e., county-level vs. census block group (CBG)-level baseline disease rates) on estimated pollution-attributable health risks.

The San Francisco Bay Area of California has a population of >7 million people. This case study for the Bay Area, where high-resolution concentration and disease rate data are available, allows us to explore intra-urban disparities in air pollutant exposure, pollution-attributable health risks, and pollution-attributable disease burdens—three related but distinct metrics that are used in policy contexts. The objectives of our study were to *a*) identify the degree of spatial heterogeneity in air pollution-related health impacts at the neighborhood scale within a city; *b*) compare the spatial patterns of air pollution disease burdens estimated using different concentration and baseline disease rate data sets; and *c*) draw lessons learned for conducting neighborhood-scale air pollution health impacts in cities where highly resolved concentration and baseline disease rate data sets are not available. We anticipate that our results can be used to inform best practices (currently under development) for assessing air pollution-related health risks within cities globally, as well as efforts by policymakers to address disparities in the health impacts of air pollution.

Methods

We used epidemiologically derived health impact functions to estimate mortality and morbidity that may be attributable to NO_2, BC, and $PM_{2.5}$, on a 100-m grid resolution for the Bay Area, using different concentration inputs and varying spatial resolutions for baseline disease rates. We used the Bay Area Air Quality Management District's (BAAQMD) nine-county definition of the Bay Area, which included Alameda, Contra Costa, Marin, Napa, San Francisco, Santa Clara, San Mateo, Solano, and Sonoma counties (Figure 1). Within the Bay Area, we focused on Alameda County, for which we were able to obtain CBG-level disease rates, and within Alameda County, the areas of West, Downtown, and East Oakland, where the Street View cars measured pollution levels (Table 1). Oakland is home to a major container port and has four large interstates (I-880 to the south and west; I-80 and I-580 to the north; and I-980 transecting West and Downtown Oakland), as well as numerous rail yards and rail lines. East and West Oakland have been designated by the California Environmental Protection Agency (EPA) Environmental Justice Task Force as priority communities bearing disproportionate pollution burdens (Environmental Justice Task Force 2017).

Health Impact Function

For each pollutant–outcome pair, we derived concentration–response factors (CRFs) from relative risk (RR) estimates (Table 1) identified through a literature review using PubMed and Google Scholar (see the Supplemental Material "Literature Review" and Tables S1–S15 and Figures S1–S11). We used epidemiological studies with large geographic areas as opposed to those conducted in single cities, assuming large epidemiological studies more fully account for population variation and confounding factors and have more statistical power. Where available, we used pooled risk estimates from meta-analyses. We applied a log-linear function to all analyses, based on current evidence for $PM_{2.5}$ and, for NO_2, a combination of limited evidence for linear vs. log-linear functions and only small differences between the two at the concentrations in our study. Equation 1 describes the log-linear health impact function used for all pollutant–health end point pairs:

$$y_{h,i,a} = m_{h,i,a} \times P_{i,a} \times (1 - e^{-\beta_{h,a}\Delta x_i}) \quad (1)$$

where $y_{h,i,a}$ represents the number of cases of the health outcome (h) for age group (a) attributable to the pollutant for each grid cell (i); $m_{h,i,a}$ represents the baseline disease rate for each health end point (h), age group (a), and grid cell (i); $P_{i,a}$ represents the population count for each grid cell (i) and age group (a); and $1 - e^{-\beta_{h,a}\Delta x_i}$ represents the attributable fraction, with $\beta_{h,a}$ the natural log of the RR per x concentration above the baseline (Δx) in each grid cell (i), for each health end point (h) and age group (a). We accounted for uncertainty by calculating the attributable cases at the 2.5th and 97.5th percentiles of the RR estimates. All health

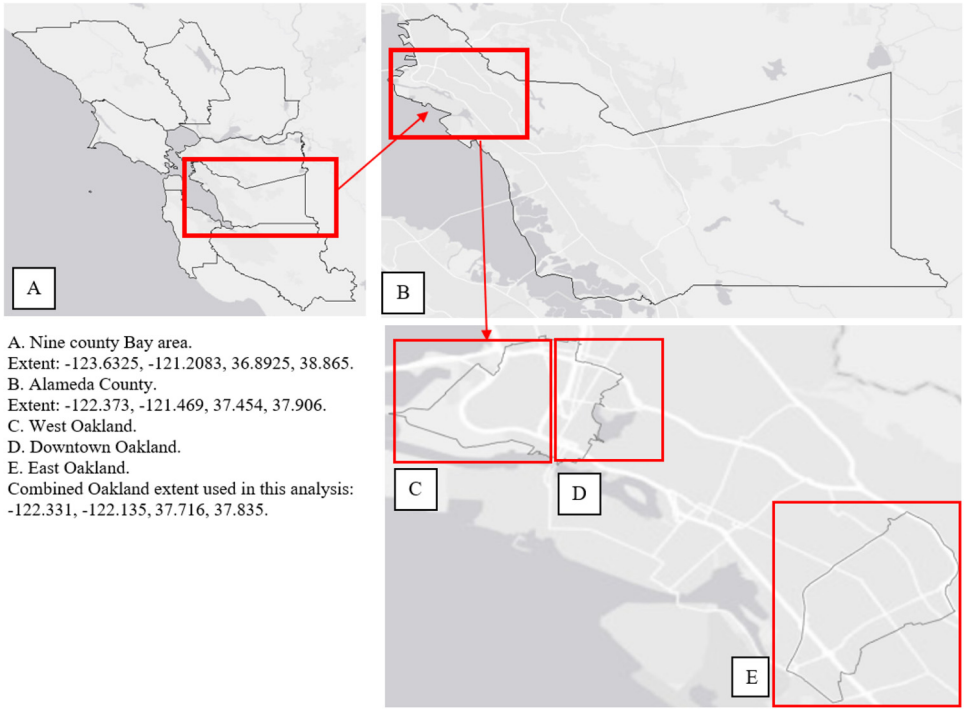

Figure 1. Geographic area of analysis for (A) the Bay Area, California, highlighting (B) Alameda County and (C) West, (D) Downtown, and (E) East Oakland within Alameda County. Base map data from ArcMap (version 10.4; Esri), HERE, Garmin, FAO, NOAA, USGS, © OpenStreetMap contributors, and the GIS User Community.

impact calculations were conducted in R (version 3.5.3; R Development Core Team).

For all pollutants, we assumed no threshold for low concentrations because a recent study identified health impacts at $PM_{2.5}$ concentrations as low as $2\,\mu g/m^3$ (Crouse et al. 2012) and a recent NO_2 epidemiological study included concentrations as low as 2 ppb (Khreis et al. 2017). Given that we applied a log-linear function to both $PM_{2.5}$ and BC, we likewise assumed no threshold for BC. For NO_2, the U.S. EPA (2016) determined that there are causal and likely causal relationships for short-term and long-term exposure and respiratory effects, respectively. Because we were able to obtain baseline disease rates for pediatric asthma emergency room (ER) visits and pediatric asthma incidence, two of which included respiratory outcomes included in the U.S. EPA's "Integrated Science Assessment for Nitrogen Oxides" (U.S. EPA 2016), we included these health end points for short- and long-term exposure to NO_2. Recent meta-analyses have also determined that there is a likely causal relationship between long-term exposure to NO_2 and increased risk of mortality (COMEAP 2018) and potentially for CVD mortality, the most commonly included cause-specific mortality end point among included studies in the meta-analysis (Atkinson et al. 2018). We estimated impacts of NO_2 on all-cause and CVD mortality. Although we examined NO_2, there remains active debate on the independent causal relationship between long-term NO_2 on mortality and other health outcomes. NO_2 is, however, a well-established marker of localized traffic-related air pollution, such as ultrafine particles and polycyclic aromatic hydrocarbons and is used as a proxy to estimate the mortality burden due to highly variable local traffic-related air pollution (Atkinson and Butland 2018) important for urban air pollution policy decision making.

For $PM_{2.5}$, we included health end points determined to be causal or likely to be causal by the U.S. EPA, including all-cause mortality, CVD mortality, CVD hospitalizations among the elderly, and pediatric asthma incidence and ER visits (U.S. EPA 2019). For BC, the U.S. EPA concluded that there is currently insufficient evidence to ascribe any one component of $PM_{2.5}$ as more strongly associated than total $PM_{2.5}$ mass, although some studies found associations between long-term exposure to BC and all-cause and CVD mortality, and between short-term BC exposure and CVD hospitalizations (U.S. EPA 2019). We therefore included all-cause and CVD mortality, as well as CVD hospitalizations for BC. Because applying the log-linear model to individual $PM_{2.5}$ components can distort the risk estimates given nonlinearity at the low end of the curve (Anenberg et al. 2012), we performed a sensitivity analysis in which we assumed the BC contribution to $PM_{2.5}$ mortality was the same as its contribution to $PM_{2.5}$ concentrations.

NO_2, BC, and $PM_{2.5}$ Concentrations

We used multiple pollutant concentration data sets, including mobile monitoring (BC and NO_2) and predictive models for the United States and globally using an LUR model (NO_2), and for the United States (BC and $PM_{2.5}$) and globally ($PM_{2.5}$) using satellite-based models. Maps of concentrations for each pollutant, data set source, and geographical extent are provided in Figures S12–S28.

For the mobile monitoring data set, two Street View cars equipped with fast-response instrumentation [NO_2 via cavity attenuation phase shift spectroscopy (Model T500U, Teledyne Inc.), and BC via photoacoustic absorption spectroscopy (Droplet Measurement Technologies)] repeatedly drove every road in West, Downtown, and East Oakland during daytime hours ($\sim$0900–1800 hours) on weekdays between 28 May 2015 and 21 December 2017, producing >3 million data points (Apte et al. 2017; Aclima et al. 2019). These measurements were aggregated to independent drive pass means, and then medians of the drive pass means were calculated for 30-m road segments, reflecting long-term spatial differences in concentrations (Messier et al.

Table 1. Relative risks (RRs) used for estimating the health impacts (95% CIs in parentheses) and inputs used for calculating each pollutant–health outcome pair.

Pollutant	Concentrations	Health outcome	Baseline disease rates	Age group	Study	RR (95% CI)
BC	Street view for Oakland and van Donkelaar et al. 2019 for Bay Area	All-cause mortality	Alameda County: CBG level Bay Area: county level	Adults	Janssen et al. 2011	1.007 (1.004, 1.009)
		CVD mortality	Alameda County: CBG level Bay Area: county level	Adults	Janssen et al. 2011	1.018 (1.011, 1.031)
		CVD hospitalizations	Bay Area: county level	Elderly	Peng et al. 2009	1.020 (1.008, 1.032)
NO_2	Street View for Oakland, Larkin et al. 2017 (main results) and Bechle et al. 2015 (sensitivity) for Bay Area	All-cause mortality	Alameda County: CBG level Bay Area: county level	Adults	Atkinson and Butland 2018	1.040 (1.011, 1.069)
			Alameda County: CBG level Bay Area: county level	Adults	Crouse et al. 2015	1.1025 (1.082, 1.145)
			Alameda County: CBG level Bay Area: county level	Elderly	Eum et al. 2019	1.023 (1.021, 1.026)
		CVD mortality	Alameda County: CBG level Bay Area: county level	Adults	Atkinson et al. 2018	1.006 (1.004, 1.009)
			Alameda County: CBG level Bay Area: county level	Elderly	Eum et al. 2019	1.103 (1.099, 1.108)
		Asthma incidence	State level for California	Pediatric	Khreis et al. 2017	1.258 (1.098, 1.374)
		Asthma ER visits	Bay Area: ZIP-code level	All ages	Orellano et al. 2017	1.024 (1.005, 1.043)
			Bay Area: ZIP-code level	All ages	Zheng et al. 2015	1.002 (1.001, 1.003)
			Bay Area: ZIP-code level	Pediatric	Orellano et al. 2017	1.040 (1.001, 1.081)
			Bay Area: ZIP-code level	Pediatric	Zheng et al. 2015	1.003 (1.002, 1.004)
$PM_{2.5}$	van Donkelaar et al. 2016 (main results) and Di et al. 2016 (sensitivity) for Bay Area	All-cause mortality	Alameda County: CBG level Bay Area: county level	Adults	Krewski et al. 2009	1.06 (1.04, 1.08)
			Alameda County: CBG level Bay Area: county level	Elderly	Di et al. 2017	1.084 (1.081, 1086)
		CVD mortality	Alameda County: CBG level Bay Area: county level	Adults	Turner et al. 2016	1.12 (1.09, 1.15)
			Alameda County: CBG level Bay Area: county level	Elderly	Thurston et al. 2016	1.100 (1.050, 1.150)
		CVD hospitalizations	Bay Area: county level	Elderly	Bravo et al. 2017	1.008 (1.006, 1.010)
		Asthma incidence	State level for California	Pediatric	Khreis et al. 2017	1.344 (1.105, 1.629)
		Asthma ER visits	Bay Area: ZIP-code level	Pediatric	Lim et al. 2016	1.048 (1.028, 1.067)

Note: RRs are reported per 10 $\mu g/m^3$ for $PM_{2.5}$, per 10 ppb for NO_2, and per 1 $\mu g/m^3$ for BC. RRs for NO_2 reported per 10 $\mu g/m^3$ were converted to RR per 10 ppb assuming ambient air pressure of 1 atmosphere and temperature of 25° C. Adults, 25–99 years of age; BC, black carbon; CBG, census block group; CI, confidence interval; CVD, cardiovascular disease; elderly, 65–99 years of age; ER, emergency room; NO_2, nitrogen dioxide; $PM_{2.5}$, fine particulate matter; pediatric, 0–17 years of age.

2018). The resulting data set indicated substantial spatial variability at fine scales, with median concentrations for road segments within the same city blocks observed to vary by up to a factor of five. Here, we further aggregated the 30-m segment averages to a 100 m × 100 m grid resolution using a mean of all the mobile measurement points in each grid cell. This resulted in a concentration data set with an annual average NO_2 concentration range of 3.37 to 45 ppb [mean = 12.7, standard deviation (SD) = 6.6] and annual average BC concentration range of 0.2 (limit of detection) to 2.59 $\mu g/m^3$ (mean = 0.47, SD = 0.35).

For NO_2, LUR models offer full spatial coverage in addition to the very high spatial resolution needed to capture near-roadway concentrations (Hystad et al. 2011). Here, we used a global LUR that estimated annual average NO_2 at 100 m × 100 m resolution for 2011 using satellite measurements, numerous land-use predictor variables, and annual measurement data from 5,220 air monitors in 58 countries (Larkin et al. 2017). The resulting NO_2 concentrations for 2011 in the Bay Area ranged from 1 to 37 ppb (mean = 8, SD = 4), and the model explained 54% (adjusted R^2 of 0.54) of the variance in global NO_2 concentrations, with an absolute mean error of 3.7 ppb. This data set has been applied in recent health impact assessments quantifying the global burden of NO_2 on pediatric asthma incidence (Achakulwisut et al. 2019). Because the global LUR model was not calibrated specifically for the United States, we also estimated results using a U.S.-specific LUR (Bechle et al. 2015). Results from the Street View concentrations were not included in the global LUR; therefore, we do not expect spatial distributions in concentrations to match. We reported estimates using the global LUR as the main results to inform best practices for neighborhood-scale health impact assessments in cities globally.

Although $PM_{2.5}$ was not measured by the Street View cars, $PM_{2.5}$ is more spatially homogenous compared with NO_2 and can therefore be estimated using more coarsely resolved predictive models. Therefore, we used surface concentrations derived from satellite observations of AOD from both global (van Donkelaar et al. 2016) and U.S.-specific models (van Donkelaar et al. 2019; Di et al. 2016). The global $PM_{2.5}$ data set [0.01 × 0.01 (~ 1 km^2)-degree resolution] combined AOD from three satellite products, Goddard Earth Observing System (GEOS)-Chem chemical transport modeling, and geographically weighted regression to merge surface monitor *in situ* measurements of $PM_{2.5}$. The model accounted for 81% of the variance in $PM_{2.5}$ and resulted in annual average surface $PM_{2.5}$ concentrations ranging from 3 to 18.5 $\mu g/m^3$ (mean = 9, SD = 2.8) across the Bay Area for 2016. The global $PM_{2.5}$ data set was inclusive of BC, although the authors recently developed a North American product, employing similar methods to estimate $PM_{2.5}$ and speciated components of $PM_{2.5}$ also at 0.01 × 0.01-degree resolution. Although U.S. estimates for BC explained 68% of the total variance in BC, estimates for BC in the U.S. Northwest are considerably lower (R^2 = 0.29). For the North American data set in the Bay Area for 2016, BC concentrations for 2016 ranged from 0.1 to 0.7 $\mu g/m^3$ (mean = 0.3, SD = 0.1) and $PM_{2.5}$ was slightly lower than the global model with concentrations ranging from 2.9 to 11 $\mu g/m^3$ (mean = 5.9, SD = 1.5). For $PM_{2.5}$, we compared health burden estimates using global satellite-derived estimates to North American satellite-derived estimates, whereas for BC, our main analysis compared the satellite-derived model to Street View mobile monitoring concentrations. Given that satellite-derived $PM_{2.5}$ concentrations are highly uncertain (Diao et al. 2019), we also estimated results using a more statistically based $PM_{2.5}$ model for the United States (Di et al. 2016, 2017).

Baseline Disease Rates and Demographics

Maps of baseline disease rates for all health end points and spatial resolutions are provided in Figures S29–S35. We obtained all-cause and CVD mortality rates at both the CBG and county levels (Table S16). For the CBG level, we obtained counts and rates for all-cause and CVD mortality [categorized according to the *International Statistical Classification of Diseases, 10th Revision* (ICD-10; WHO 2016) ICD-10 codes I10–I75] from the Alameda County Public Health Department for adults and the elderly. CBG rates were based on 7-y averages of death counts (2011–2017) over average population counts for 2012, 2014, and 2016 (Eayres and Williams 2004) and were age-adjusted using the standard 2000 U.S. Census population (Pickle and White 1995). In addition, CBGs with counts <10 were suppressed to protect confidentiality (Brillinger 1986). Combined, these methods avoid interannual variability for small-area (CBG-level) baseline disease rates and resulted in a conservative mean relative standard error of 15 (range = 7–58, SD = 5) for 1,046 CBGs. For all-cause mortality ages ≥25 y, there were 6 (0.5%) missing block groups, and for all-cause mortality ages ≥65 y, there were 9 (0.86%) missing block groups. For CVD mortality, there were 37 (3.53%) missing block groups for ages ≥25 y and 71 (6.79%) missing block groups for ages ≥65 y. To impute missing CBG baseline disease rates, we used an average of the five nearest neighbor rates. We obtained age-adjusted county-level mortality data for 2016 for both all-cause and CVD mortality most closely matching our CBG disease categories (ICD-10 codes I00–I78) from CDC Wonder (CDC 2018). CBG baseline mortality rates show more heterogeneity in the spatial distribution of disease. Annual all-cause mortality for adults ranged from 29 to 331 per 10,000, compared with 21 to 38 per 10,000 using the county rates.

We were unable to obtain baseline disease rates at the CBG level for nonmortality end points. For CVD hospitalizations rates, we used county-level rates from the BenMap-CE 1.4.14 (BenMap) software produced by the U.S. EPA for conducting health impact assessment (Sacks et al. 2018). Rates were available in BenMap for the elderly in 5-y age groups: ages 65–69, 70–74, 75–79, 80–84, and 85–99 y. The BenMap program uses 2010 U.S. Census data as the denominator when pooling age groups into a single rate. We applied the 5-y age group rates to the 10-y age groups (65–74, 75–84, and ≥85 y) available from the 2010 U.S. Census and used the U.S. Census data from BenMap as the denominator. We weighted the rates by age group count and created an aggregated rate per county ($n = 9$) for CVD hospitalizations. CVD hospitalization (ICD-9 codes 390–429) rates in 2014 ranged from 296 to 604 per 10,000 for ages 65–99 y, across counties in the Bay Area. For asthma ER visits (ICD-9 code 493/ICD-10 code J45), we used county-level rates and ZIP-code–level rates from the California Department of Public Health for 2016 (CDPH 2017, 2019), and we used county rates to impute data for missing ZIP-code rates (17% of the pediatric population and 10% of the adult population). Across the ZIP codes in the Bay Area, 2016 baseline rates of asthma ER visits among children ranged from 1 to 154 per 10,000, and for adults, from 1 to 175 per 10,000. For pediatric asthma incidence, we applied a California statewide baseline rate for 2008 of 107 per 10,000 persons ($n = 96{,}550$) (Milet et al. 2013) because more recent and finer resolution data were not available. Preprocessing of baseline disease rates was conducted in ArcMap (version 10.4; Esri).

We used nighttime (i.e., estimates of permanent residents) population counts from the LandScan USA data set at 100 m × 100 m resolution for 2017 given that it most closely aligned with the temporal availability of our pollutant and baseline disease rate data sets (Oak Ridge National Laboratories 2020; Bhaduri et al. 2007). Compared with the daytime population, we considered the nighttime population to be more consistent with the common approach of epidemiological studies to assign exposure based on home address. LandScan USA employed a multidimensional dasymetric modeling technique, spatially redistributing the U.S. Census data to inhabited land-use areas. Because LandScan USA does not include age breakdowns, we calculate the fraction of the total population in different age groups using age-specific counts from the Gridded Population of the World (version 4) for 2010, available at 1-km resolution from the Socioeconomic Data and Applications Center at the Center for International Earth Science Information Network at Columbia University (CIESEN 2019). To ascertain whether using fine-resolution baseline disease rates identifies disparities in pollutant-attributable disease between population subgroups, we estimated the percentage of pollutant-attributable cases in Alameda County in CBGs with >50% minority (Black, Asian, Hispanic, Pacific Islander, and American Indian) population, using U.S. Census population counts at the CBG level for 2010, the most recent year available.

Because our intention was to inform best practices for cities around the world to conduct within-city health impact assessments, we compared the spatial distributions of NO_2- and BC-attributable pollutant-attributable disease burdens estimated using Street View vs. globally available modeled concentrations from LUR- (Larkin et al. 2017) and satellite-based models (van Donkelaar et al. 2016). To do this comparison, we used the Getis-Ord local statistic in ArcPro (version 2.7), which provides a *Z*-score with accompanying *p*-value indicating whether each area has estimated pollutant-attributable cases that are higher or lower than surrounding grid cells (Ord and Getis 1995). We also compared the influence of CBG vs. county-level disease rates on the spatial patterns of estimated air pollution-related all-cause mortality in Alameda County given that baseline disease rates are not typically available at the CBG scale.

We also conducted several policy-relevant sensitivity analyses to assess the pollutant-attributable health impacts that could be avoided if air pollutant concentrations were reduced to lower levels. We specifically assessed two hypothetical scenarios in which concentrations of each pollutant were reduced to the minimum and median grid-cell–level concentrations of each data set. These scenarios are conceptually similar to pollution reduction targets for West Oakland established in the West Oakland Community Action Plan (BAAQMD and West Oakland Environmental Indicators Project 2019) as part of efforts by the State of California to identify and reduce air pollution among disproportionately exposed California communities, as required by 2017 Assembly Bill 617 (Cal AB 617 2017).

Results

Overall Pollutant-Attributable Disease Burdens in the Bay Area

We first estimated the total burden of NO_2, BC, and $PM_{2.5}$ across the Bay Area using the spatially complete concentration estimates from the global LUR and satellite-based models and county-level disease rates (Table 2–4). We estimated that 2,520 [95% confidence interval (CI): 740, 4,190], 150 (95% CI: 80, 190), and 3,080 (95% CI: 2,100, 4,020) deaths could be attributable to NO_2, BC, and $PM_{2.5}$ annually in the Bay Area, respectively. We also estimated asthma morbidity attributable to NO_2 and $PM_{2.5}$ across the Bay Area. Using a state-level asthma incidence rate and ZIP-code–level asthma ER visits, we estimated 5,210 (95% CI: 2,340, 6,780) and 5,590 (95% CI: 2,120, 8,250) new pediatric asthma cases, and 620–730 (95% CI: 20, 1,400) and 720 (95% CI: 430, 990) asthma ER visits attributable to NO_2 and $PM_{2.5}$ annually in the Bay Area, respectively. For NO_2 and $PM_{2.5}$, for which we had both U.S. and global concentration models, we

Table 2. Health impact model inputs and estimated pollutant-attributable cases of various health outcomes for nitrogen dioxide (NO_2) for the Bay Area.

				Total burden using concentrations from Larkin et al. (2017)		Burden remaining after reduction to median concentrations (11.6 ppb)		Total burden reduced using median concentrations (%)	Burden remaining after reduction to minimum concentrations (1 ppb)		Total burden reduce using minimum concentrations (%)
NO_2	Concentration–response function	Age groups	Baseline disease rate resolution	Attributable cases per 100,000	Attributable cases	Attributable cases per 100,000	Attributable cases		Attributable cases per 100,000	Attributable cases	
All-cause mortality	Atkinson and Butland 2018	Adults	County	50 (10, 80)	2,520 (740, 4,190)	30 (10, 50)	1,380 (400, 2,330)	45	3 (1, 10)	180 (50, 300)	93
	Eum et al. 2019	Elderly	County	110 (100, 120)	1,020 (930, 1,150)	60 (60, 70)	570 (520, 640)	44	10 (10, 10)	70 (70, 80)	93
CVD mortality	Atkinson et al. 2018	Adults	County	20 (10, 30)	1,100 (740, 1,760)	12 (8, 19)	610 (410, 980)	45	2 (1, 2)	80 (50, 130)	93
	Eum et al. 2019	Elderly	County	150 (140, 160)	1,410 (1,360, 1,470)	90 (80, 90)	800 (770, 840)	43	10 (10, 10)	110 (100, 110)	93
Asthma incidence	Khreis et al. 2017	Pediatric	State of California	300 (140, 390)	5,210 (2,340, 6,780)	180 (80, 240)	3,070 (1,310, 4,110)	41	20 (10, 30)	420 (170, 580)	92
Asthma ER visits	Orellano et al. 2017	All ages	ZIP code	30 (10, 60)	2,420 (520, 4,230)	20 (0, 30)	1,270 (270, 2,250)	45	2 (0, 5)	160 (30, 290)	93
		Pediatric	ZIP code	40 (0, 80)	730 (20, 1,400)	20 (0, 50)	400 (10, 780)	47	3 (0, 10)	50 (0, 100)	93
	Zheng et al. 2015	All ages	ZIP code	30 (20, 40)	2,480 (1,540, 3,400)	20 (10, 20)	1,300 (810, 1,800)	45	2 (1, 3)	170 (100, 230)	93
		Pediatric	ZIP code	40 (30, 50)	620 (450, 790)	20 (10, 30)	340 (250, 440)	47	3 (2, 3)	40 (30, 60)	93

Note: Values in parentheses indicate 95% confidence intervals based on the error in the relative risk estimates only. Adults, 25–99 years of age; CVD, cardiovascular disease; elderly, 65–99 years of age; ER, emergency room; pediatric, 0–17 years of age.

Table 3. Health impact model inputs and estimated pollutant-attributable cases of various health outcomes for the Bay Area.

				Total burden using concentrations from van Donkelaar et al. (2019)		Median concentrations (0.3 μg/m^3)		Total burden reduced using median concentrations (%)	Minimum concentrations (0.1 μg/m^3)		Total burden reduce using minimum concentrations (%)
BC	Concentration–response function	Age groups	Baseline disease rate resolution	Attributable cases per 100,000	Attributable cases	Attributable cases per 100,000	Attributable cases		Attributable cases per 100,000	Attributable cases	
All-cause mortality	Janssen et al. 2011	Adults	County	3 (2, 4)	150 (80, 190)	2 (1, 2)	90 (50, 120)	37	1 (0, 1)	30 (20, 40)	78
CVD mortality	Janssen et al. 2011	Adults	County	1 (0, 1)	50 (30, 60)	1 (0, 1)	30 (20, 40)	38	0 (0, 0)	10 (5, 10)	78
CVD hospitalizations	Peng et al. 2009	Elderly	County	40 (10, 60)	340 (130, 530)	20 (10, 40)	210 (80, 340)	36	10 (0, 10)	70 (30, 120)	78

Note: Values in parentheses indicate 95% confidence intervals based on the error in the relative risk estimates only. Adults, 25–99 years of age; BC, black carbon; CVD, cardiovascular disease; elderly, 65–99 years of age.

Table 4. Health impact model inputs and estimated pollutant-attributable cases of various health outcomes for fine particulate matter ($PM_{2.5}$) for the Bay Area.

$PM_{2.5}$	Concentration–response function	Age groups	Baseline disease rate resolution	Total burden using concentrations from van Donkelaar et al. 2016		Median concentrations (10 μg/m³)		Total burden reduced using median concentrations (%)	Minimum concentrations (3 μg/m³)		Total burden reduce using minimum concentrations (%)
				Attributable cases per 100,000	Attributable cases	Attributable cases per 100,000	Attributable cases		Attributable cases per 100,000	Attributable cases	
All-cause mortality	Krewski et al. 2009	Adults	County	60 (40, 80)	3,080 (2,100, 4,020)	50 (30, 60)	2,500 (1,700, 3,280)	19	20 (10, 20)	790 (530, 1,030)	74
	Di et al. 2017	Elderly	County	310 (300, 310)	2,920 (2,820, 2,980)	250 (240, 260)	2,400 (2,320, 2,450)	18	80 (80, 80)	760 (730, 780)	74
CVD mortality	Turner et al. 2016	Adults	County	40 (30, 40)	1,790 (1,390, 2,170)	30 (20, 40)	1,470 (1,130, 1,790)	18	10 (10, 10)	470 (360, 580)	74
	Thurston et al. 2016	Elderly	County	120 (60, 170)	1,160 (610, 1,650)	100 (50, 140)	950 (500, 1,360)	18	30 (20, 50)	300 (160, 440)	74
CVD hospitalizations	Bravo et al. 2017	Elderly	County	40 (30, 50)	360 (280, 430)	30 (20, 40)	290 (220, 350)	19	10 (10, 10)	90 (70, 110)	75
Asthma incidence	Khreis et al. 2017	Pediatric	State of California	320 (120, 480)	5,590 (2,120, 8,250)	270 (100, 410)	4,640 (1,710, 7,000)	17	90 (30, 150)	1,560 (540, 2,510)	72
Asthma ER visits	Lim et al. 2016	Pediatric	ZIP code	40 (30, 60)	720 (430, 990)	30 (20, 50)	590 (350, 800)	19	10 (10, 20)	180 (110, 250)	75

Note: Values in parentheses indicate 95% confidence intervals based on the error in the relative risk estimates only. Adults, 25–99 years of age; CVD, cardiovascular disease; elderly, 65–99 years of age; ER, emergency room; pediatric, 0–17 years of age; $PM_{2.5}$, particulate matter ≤2.5 μm in aerodynamic diameter.

estimated 30% and 37% larger annual attributable mortality burdens using the global vs. U.S. concentration data sets (NO_2 global = 2,520; NO_2 U.S. = 1,930; $PM_{2.5}$ global = 3,080; $PM_{2.5}$ U.S. = 1,960 = Excel Tables S1 and S2), consistent with the magnitude difference in concentration estimates.

Estimated 100-m grid-cell–level pollution-attributable mortality rates (annual attributable deaths per 100,000 people) ranged across the Bay Area by a factor 38, 4, and 5 for NO_2, BC, and $PM_{2.5}$ (NO_2 range = 3–113, mean = 30, SD = 13; BC range = 1–4, mean = 2, SD = 1; $PM_{2.5}$ range = 20–95, mean = 49, SD = 13; Excel Tables S1–S3). For NO_2, the largest mortality impact among counties occurred in Alameda County, where it was 14 times larger than in the least impacted county, Napa (Bay Area county range = 40–570 attributable deaths annually, mean = 280, SD = 210; city range = 0–390, mean = 11, SD = 38; Excel Tables S4 and S5). Inter-county and -city variation in BC-attributable mortality was also high, with Santa Clara County having a burden 13 times that of Napa County (county range = 3–40 attributable deaths annually, mean = 16, SD = 12; city range = 0–20, mean = 1, SD = 2; Excel Tables S6 and S7). For $PM_{2.5}$, the most impacted county (Santa Clara) had a $PM_{2.5}$ mortality burden that was 12 times larger than the least impacted county (Napa) (county range = 60–690 attributable deaths annually, mean = 340, SD = 230; city range = 0–395, mean = 14, SD = 40; Excel Tables S8 and S9).

Influence of Varying Pollutant Concentrations Data Sets and Baseline Disease Rates

We next focused in on West, Downtown, and East Oakland ($\sim 30\ km^2$), the part of the Bay Area where Street View measurements of NO_2 and BC are available and can be compared with the application of concentrations from predictive models. Total estimated NO_2-attributable deaths in Oakland approximately doubled when using the LUR [77 annual attributable deaths (95% CI: 23, 127)] compared with the Street View concentrations [39 (95% CI: 12, 66)] (Figure 2). NO_2-attributable mortality rates ranged across 100-m grid cells by a factor of 11 and 26 using LUR and Street View estimates, respectively (LUR range = 32–342 annual attributable deaths per 100,000, mean = 101, SD = 31; Street View range = 15–396, mean = 64, SD = 39).

BC-attributable mortality burdens using concentrations from the predictive model (van Donkelaar et al. 2019) exceeded the estimates based on Street View concentrations in Oakland [Street View = 2 annual attributable deaths (95% CI: 1, 3); satellite-derived: 4 (95% CI: 2, 5)]. For BC and $PM_{2.5}$, pollution-attributable mortality rates ranged across 100-m grid cells by a factor of 39, 12, and 8 when using BC Street View, U.S. BC satellite-derived, and global $PM_{2.5}$ satellite-derived concentrations, respectively (range = 0–39 annual attributable deaths per 100,000, mean = 4, SD = 4; range = 1–12, mean = 5, SD = 1; range = 22–183, mean = 96, SD = 29). In our sensitivity analysis using a proportional approach that assumed that the BC contribution to $PM_{2.5}$ mortality is the same as its contribution to $PM_{2.5}$ concentrations (1.25–7.5% using the satellite-derived concentration estimates), the range of the BC-attributable fraction of mortality across 100-m grid cells was very similar to our core results (0.07–0.5%, applying the log-linear CRF to BC, and 0.06–0.4%, using the proportional approach).

Despite moderate-to-low correlation between concentrations from the Street View monitoring and predictive models, we found similar spatial clusters of NO_2 and BC-attributable fractions using both concentration data sets. For the grid cells in the Oakland area for which we had both Street View and LUR (NO_2) and U.S. satellite-derived (BC) results, a large fraction of grid cells (NO_2: 45%, $n = 1{,}619$; BC: 37%, $n = 1{,}334$) were fully concordant using

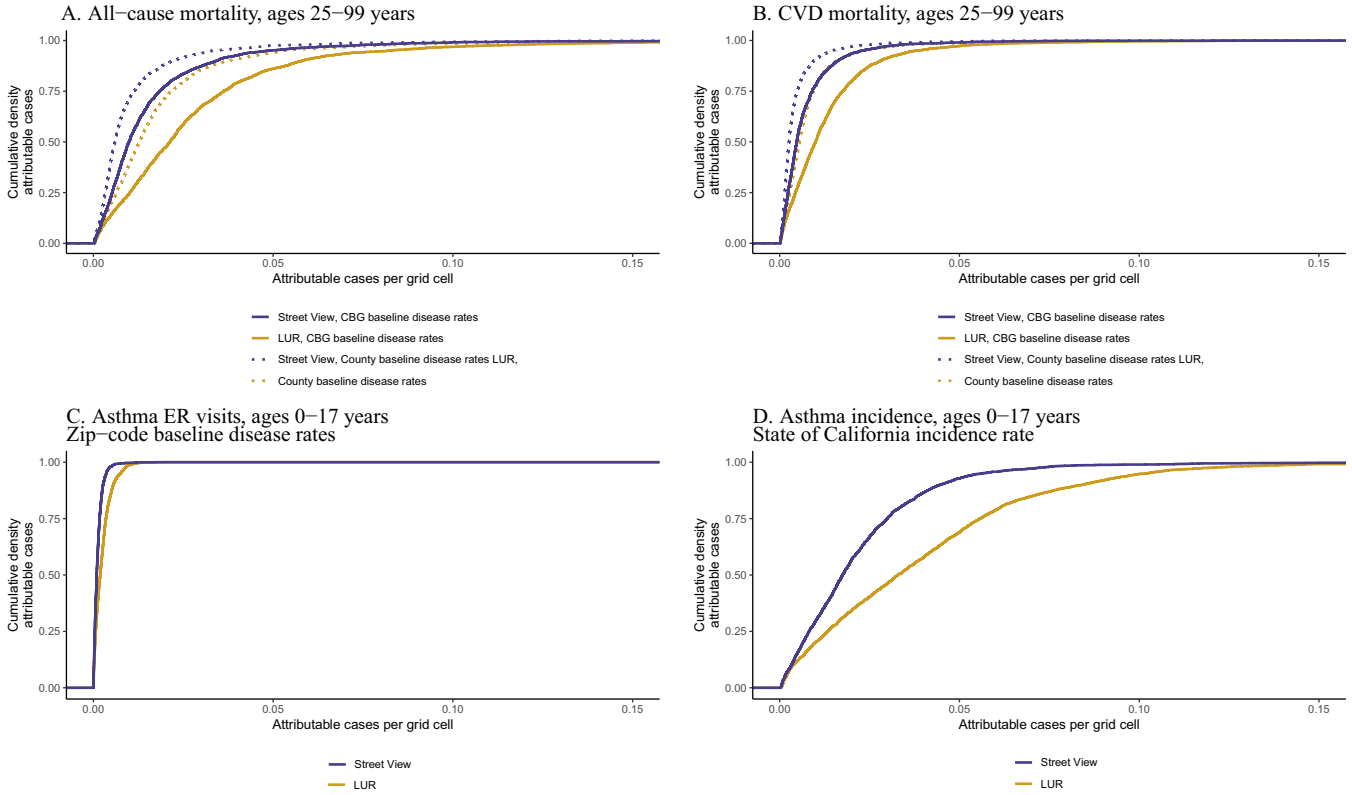

Figure 2. Cumulative density of annual nitrogen dioxide (NO_2)-attributable cases per 100 m × 100 m grid cell in Oakland, California, using different concentration and baseline disease rate data sets. (A) All-cause mortality, ages 25–99 y; (B) cardiovascular disease mortality, ages 25–99 y; (C) asthma ER visits, ages 0–17 y, ZIP-code baseline disease rates; and (D) asthma incidence, ages 0–17 y, State of California incidence rate. Note: ER, emergency room.

the *Z*-score statistic, meaning that both concentration data sets identified clusters of attributable cases that are both significant ($p < 0.05$) and in the same direction (either a higher or lower value cluster) (Figures S36 and S37). Another 37% ($n = 1{,}309$) and 22% ($n = 799$) of grid cells for NO_2 and BC had directional concordance, but concentration data sets identified differing significance in the clusters. We also found that 13% ($n = 452$) and 15% ($n = 546$) of grid cells for NO_2 and BC, respectively, were directionally discordant between the two concentration data sets but had the same significance level. About 5% ($n = 193$) and 25% ($n = 899$) of grid cells for NO_2 and BC were completely discordant. Although both data sets identified similar hotspots, the Street View data set identified a wider range of *Z*-scores (NO_2 range = −3.98 to 10.02, mean = −0.06, SD = 2.42; BC range = −3.80 to 12.77, mean = −0.09, SD = 2.20) as compared with LUR and satellite-derived concentrations (NO_2 range = −4.07 to 7.51, mean = 0.19, SD = 2.17; BC range = −8.46 to 2.53, mean = −0.04, SD = 2.06).

We next assessed the influence of CBG vs. county-level baseline disease rates on estimated pollutant-attributable mortality within Alameda County, where we had baseline all-cause mortality rates for both spatial resolutions. Using the same modeled concentrations of NO_2 (LUR) and $PM_{2.5}$ (satellite-derived) in both cases, CBG baseline disease rates yielded 15% and 13% higher spatially aggregated estimates of pollutant-attributable mortality rates compared with the application of county baseline disease rates (NO_2 CBG = 60 annual attributable deaths per 100,000; NO_2 county = 52; $PM_{2.5}$ CBG = 70; $PM_{2.5}$ county = 61). Differences were even more evident at finer spatial aggregations. For example, for just the Oakland area extent, CBG baseline disease rates yielded 52%, 67%, and 57% higher NO_2, BC, and $PM_{2.5}$-attributable all-cause mortality rates compared with the application of county baseline disease rates (NO_2 CBG = 97 annual attributable deaths per 100,000; NO_2 county = 64; BC CBG = 5; BC county = 3; $PM_{2.5}$ CBG = 88; $PM_{2.5}$ county = 56). Applying CBG baseline disease rates also revealed spatial heterogeneity in estimated pollutant-attributable mortality rates that was masked when using county-level disease rates. Applying CBG baseline disease rates yielded grid-cell–level pollutant-attributable rates that varied by factors of 29, 12, and 14 for NO_2, BC, and $PM_{2.5}$ (NO_2 CBG range = 15–434 annual attributable deaths per 100,000, mean = 41, SD = 19; BC CBG range = 1–12, mean = 2, SD = 1; $PM_{2.5}$ CBG range = 19–267, mean = 59, SD = 17; Excel Tables S9–S12) across Alameda County, whereas applying county baseline disease rates yielded less spatial heterogeneity (6, 4, and 3 times, respectively; NO_2 county range = 19–113 annual attributable deaths per 100,000, mean = 38, SD = 11; BC county range = 1–4, mean = 2, SD = 1; $PM_{2.5}$ county: range = 32–81, mean = 55, SD = 8).

We next estimated the percentage of pollutant-attributable mortality and morbidity cases in CBGs with >50% minority population. We found that using CBG instead of county baseline disease rates resulted in a larger percentage of pollutant-attributable cases for CBGs with >50% minority population in Alameda County (Table S17 and Figures S38–S40). For example, using CBG disease rates, we estimated that 75% of NO_2-attributable mortality occurred in majority minority CBGs, whereas that percentage was 72% when using county-level disease rates. The differences between applications of CBG vs. county-level disease rates were small but generally consistent across pollutants and health end points. Within Oakland, CBGs with the highest percentage of minorities and highest estimated NO_2-attributable mortality rates were located in West Oakland near I-880, a high-traffic–volume truck route, and in Chinatown, in the southeastern part of Downtown Oakland (Figures S41 and S42).

Policy-Relevant Reductions

Using concentrations from the global (NO_2 and $PM_{2.5}$) and U.S. (BC) model data sets for the Bay Area, we found that rolling back concentrations to the median ($NO_2 = 8$ ppb; BC $= 0.3\ \mu g/m^3$; $PM_{2.5} = 10\ \mu g/m^3$, respectively) reduced attributable deaths by 45%, 37%, and 19% [remaining deaths for $NO_2 = 1{,}380$ (95% CI: 400, 2,330); BC $= 90$ (95% CI: 50, 120); $PM_{2.5} = 2{,}500$ (95% CI: 1,700, 3,280); Tables 2–4]. Varying magnitudes of reductions in attributable deaths were due to the distribution of concentrations, with $PM_{2.5}$ concentrations comparatively right skewed. Rolling back to minimum concentrations reduced cases by 93%, 78%, and 74% for NO_2, BC, and $PM_{2.5}$, respectively [177 (95% CI: 50, 300), 32 (95% CI: 20, 40), and 790 (95% CI: 530, 1,030) remaining for 1-ppb, 0.1-$\mu g/m^3$, and 3-$\mu g/m^3$ concentrations)]. Health benefits of the reduction scenarios were more pronounced within Oakland, where pollutant-attributable mortality was reduced by 59%, 40%, and 52% for NO_2, BC, and $PM_{2.5}$, respectively, under a reduction to the median concentration [32 (95% CI: 9, 53), 2 (95% CI: 1, 3), and 56 (95% CI: 38, 74) cases remaining] and by 94%, 80%, and 95% under the reduction to the minimum concentration [4 (95% CI: 1, 7), 1 (95% CI: 0, 1), and 18 (95% CI: 12, 23) cases remaining]. Health benefits were smaller when using Street View concentrations for NO_2, with a 13% and 66% decrease in NO_2-attributable mortality under reductions to the median and minimum concentrations, respectively [34 (95% CI: 20, 57) and 13 (95% CI: 4, 23) cases for 11.59 and 3.37 ppb, respectively]. Estimates for reductions using Street View BC concentrations were not possible owing to few BC-attributable cases in Oakland (<1). The top five CBGs with the highest premature mortality burden within Oakland would have experienced an estimated 27% and 79% reduction in NO_2-attributable mortality if concentrations were reduced to median and minimum concentrations, respectively. These same five CBGs had a greater than 50% population of racial and ethnic minorities, indicating that the policy changes would disproportionately benefit minority populations.

Discussion

We estimated the spatial distribution of NO_2, BC, and $PM_{2.5}$-attributable health impacts at the neighborhood-scale within the Bay Area, California, where high spatial resolution concentrations from mobile monitoring, as well as CBG-level disease rate data sets are available. We found 38-, 4-, and 5-fold variation in mortality attributable to NO_2, BC, and $PM_{2.5}$ across grid cells in the Bay Area, indicating that pollution-attributable risks can vary considerably within individual cities. This variation was observable regardless of whether predictive models or mobile monitoring concentration data sets were used, although the mobile monitoring concentrations revealed more spatial heterogeneity. Spatial heterogeneity in air pollution-attributable health risks was more pronounced when we applied CBG rather than county-level baseline disease rates.

Depending on the concentration and baseline disease data sets used, estimated NO_2-attributable mortality in Oakland at the 100-m grid-cell level varied by a factor of 2–26, BC-attributable mortality (annual deaths per 100,000) varied by a factor of 2–39, and $PM_{2.5}$-attributable mortality varied by a factor of 2–8. We found the least heterogeneity using county baseline disease rates and concentration estimates from a global model, and the greatest variation using Street View concentrations with CBG baseline disease rates. Using concentrations from Street View mobile monitoring and predictive models yielded similar spatial patterns in air pollution-attributable health risks because baseline disease rates also play an important role. For the same reason, CBGs with the highest air pollution-attributable health risks were not necessarily those with the highest pollutant concentrations.

Comparing the influence of baseline disease rates and concentrations on spatial distribution, we found that neighborhoods with the highest air pollution-attributable health risks were not necessarily those with the highest pollutant concentrations. Each additional input to the health impact function changed the spatial distribution of the estimated health burden. For example, calculating the percent of mortality that can be attributed to air pollution incorporates only the CRF and concentrations (Figure 3A). When baseline disease rates were also incorporated to estimate attributable mortality rates (Figure 3B), spatial patterns in risk shifted to different areas within West and Downtown Oakland. Finally, when population was included to estimate pollutant-attributable disease burdens (Figure 3C), spatial patterns shifted yet again. Therefore, considering only concentrations without incorporating baseline disease rates and population distribution may not adequately capture the neighborhoods with greatest pollutant-attributable health risks and burdens. The relative importance of disease rates and concentrations on spatial heterogeneity in risk estimates depended on the data set and its spatial resolution, as well as the risk metric used (attributable fraction, attributable rate, or attributable cases).

Our aggregated estimate of 3,080 (95% CI: 2,100, 4,020) $PM_{2.5}$-attributable annual deaths in the Bay Area was approximately double a previously published estimate of 1,500 deaths attributable to $PM_{2.5}$ in San Francisco (Anenberg et al. 2019) that used satellite-derived $PM_{2.5}$ concentrations from the Global Burden of Disease Study (Shaddick et al. 2018). Our estimate was also higher than the estimate from the BAAQMD (2017) Clean Air Plan of $\sim$2,500 annual deaths attributable to anthropogenic $PM_{2.5}$ emissions, which used county-level baseline disease rates and population estimates, a Community Multiscale Air Quality Modeling model estimate of $PM_{2.5}$ and a mean of 12 different CRFs (BAAQMD 2017). Analysis of various $PM_{2.5}$ concentration estimates have indicated substantial differences in spatial patterns, complicating comparability between risk assessments (Diao et al. 2019). We also used different disease rates, concentration–response functions, and low-concentration thresholds.

Mobile monitoring offers a spatially explicit observational record but has incomplete spatial coverage. Predictive models using land-use variables and satellite remote sensing have the advantage of complete spatial coverage, but estimated concentrations are uncertain. In areas where there were overlapping Street View and predictive model data for the same pollutant (NO_2), we found higher NO_2-attributable deaths when using the LUR [77 annual deaths (95% CI: 23, 137)] compared with the Street View concentrations [39 (95% CI: 12, 66)]. Compared with concentrations, NO_2-attributable mortality rates using Street View and LUR were more correlated owing to the smoothing effect of applying the same baseline disease rates ($R = 0.67$). These results indicated that the Street View data set detects extremes in concentrations and associated health burdens that are not identified by the LUR concentration data set. Comparing these results was challenged by inherent differences in the data sets: First, NO_2 concentrations decreased between 2011, for which we had LUR concentration estimates, and 2015, when the Street View mobile monitoring occurred (Duncan et al. 2016). Second, the Street View data set captured high near-roadway exposures, whereas the LUR model represented broader spatial average concentrations with smaller decay gradients of concentrations as you move away from main thoroughfares and highways, resulting in higher concentrations in residential areas. In addition, Street View measurements were taken during the daytime, which may underestimate daily NO_2 concentrations by 15–20% given that daytime

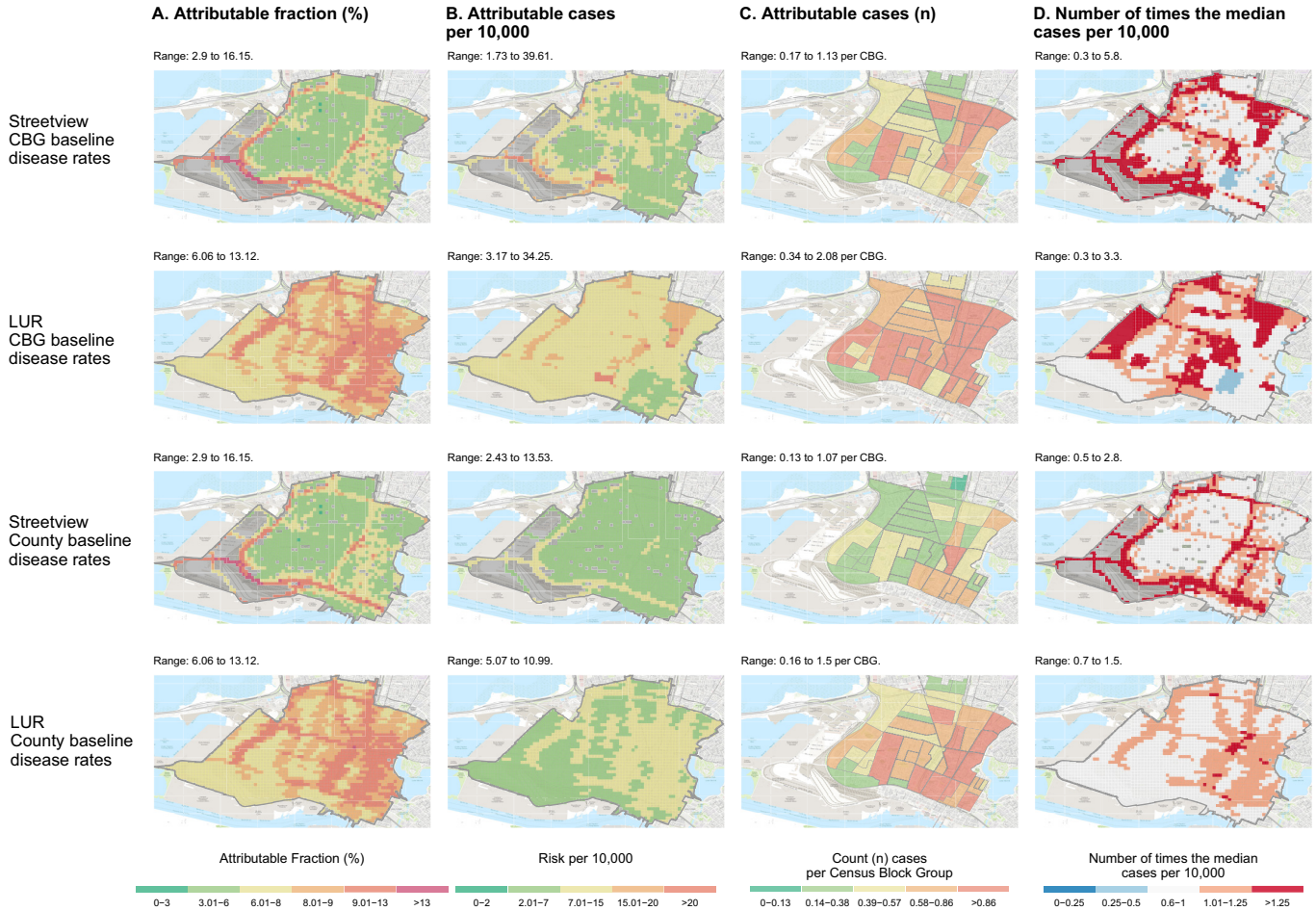

Figure 3. Spatial distribution of nitrogen dioxide (NO_2)-attributable all-cause mortality among adults in the West and Downtown Oakland area. (A) Attributable fraction; (B) attributable cases per 10,000; (C) attributable cases; and (D) number of times the median cases per 10,000. (Extent: −122.253, 477; −122.327, 816; 37.791, 334; 37.832, 312) using the Street View mobile monitoring (rows 1 and 2) and data from Larkin et al. 2017 land-use regression (LUR) (rows 3 and 4) concentration data sets, as well as census block group (CBG) (rows 1 and 3) and county (rows 2 and 4) baseline disease rates. Results depicted are for the central estimates of concentrations and relative risk estimates. Gray areas represent areas where concentration data were not available. Base map and data from OpenStreetMap and OpenStreetMap Foundation.

ambient NO_2 is depressed by photolysis. However, this effect may have been balanced by the Street View data set, which did not account for lower weekend concentrations. Given these differences, NO_2 concentrations from these two data sets were not well correlated ($R = 0.55$), and the LUR concentrations were overall higher with less spatial variability.

Our study was limited in several ways. Although concentration and population data sets are increasingly available at high resolutions, baseline disease rates are still difficult to obtain at urban and intra-urban scales. For example, for asthma incidence, we were only able to apply a statewide incidence rate, although prevalence data for asthma shows spatial heterogeneity of asthma within the Bay Area and California. Expanding disease surveillance and increasing access to highly resolved baseline disease rates in cities around the world would improve health impact assessment estimates and capacity to detect areas within cities that have elevated pollution-attributable health risks. Our analysis of racial disparities in air pollution health risks was also limited because we did not incorporate racial- and ethnicity-specific baseline disease rates or RR estimates. In addition, we applied CRFs from meta-analyses and large, nationwide cohort studies that had high quality and statistical power although their populations may not have matched the population distribution in our analysis, introducing additional unquantifiable uncertainty to our analysis.

Our pollutant-specific estimates cannot be summed together because we applied single-pollutant epidemiological models and, as such, there could be a significant amount of overlap between the deaths estimated to be attributable to each individual pollutant. Some of the relationship between NO_2 and adverse health outcomes may have been accounted for by concurrent $PM_{2.5}$ exposures, resulting in overlap of attributable deaths in our results presented for NO_2 and $PM_{2.5}$, although $PM_{2.5}$ alone does not fully capture the effects of near road traffic pollutants more strongly correlated with NO_2 (Atkinson and Butland 2018). Similarly, estimates presented here for $PM_{2.5}$ are inclusive of BC and other $PM_{2.5}$ species. Therefore, results for BC should be interpreted as a subset of $PM_{2.5}$-attributable health outcomes. We calculated results for both BC and $PM_{2.5}$ because although $PM_{2.5}$ can have multiple sources, BC is a combustion-related particle that represents the impacts of $PM_{2.5}$ traffic-related pollution as opposed to pollution form other regional sources (Janssen et al. 2011). The low magnitude of results precluded us from drawing strong conclusions from this comparison. The high spatial heterogeneity of the Street View BC concentrations resulted in poor correlation between the two data sets ($R = 0.03$), although the smoothing effect of applying the same CBG baseline disease rates to each data set resulted in increased correlation between BC-attributable mortality rates ($R = 0.36$).

The effective use of a two-pollutant CRF in health impact assessment relies upon RR estimates from studies able to meaningfully parse relationships between correlated pollutants (Dominici et al. 2010; Stafoggia et al. 2017), which were not available for most of our pollutant–health outcome pairs. For one sensitivity analysis wherein a two-pollutant model CRF for NO_2 was available, we applied a $PM_{2.5}$-adjusted RR estimate for NO_2 and CVD mortality among the elderly from the study by Eum et al. (2019), which resulted in lower total attributable case estimates (254 attributable all-cause deaths within Alameda County, using the unadjusted CRF, and 121 deaths, using the adjusted CRF), indicating a considerable portion of the burden estimated for NO_2 may be attributable to $PM_{2.5}$.

As demonstrated, pollutant concentrations varied substantially within cities, whereas air pollution cohort studies in the United States have often compared exposure between cities. No long-term North American cohort studies have analyzed within-city variation in RR estimates for $PM_{2.5}$ and all-cause mortality (Vodonos et al. 2018). The meta-analysis we employed for the relationship between NO_2 and all-cause mortality relied upon a mix of studies examining within- (i.e., the ESCAPE cohorts) and between-city (i.e., the Harvard Six Cities cohort) exposure comparisons. As a sensitivity analysis, we estimated results using a within-city RR estimate (Table 1) from a subcohort of the Canadian Census Health and Environment Cohort, which found significant relationships between NO_2 and all-cause for within-city exposure comparisons but not for between-city exposure comparisons (Crouse et al. 2015). This within-city RR estimate was also included in the meta-analysis for our main CRF (Atkinson and Butland 2018). Although the choice of CRF changed the overall magnitude of aggregated air pollution-attributable health impacts for each pollutant, it did not affect our main conclusions about the intra-urban heterogeneity because we applied the CRF uniformly across the domain. Future use of statistical methods able to assess correlated exposures (Stafoggia et al. 2017) will allow for improved application of two-pollutant model estimates health impact assessment and policy-making.

Interpreting and communicating the uncertainties in a health impact assessment is a known challenge (Nethery and Dominici 2019) because, with each input parameter to the health impact function, there is associated uncertainty. We estimated uncertainty using the CIs of the RR estimates, but we were unable to quantify uncertainty in the pollutant concentrations, baseline disease rates, and population estimates. Gridded population estimates are also increasingly available at a fine spatial resolution. Prior to selecting a population data set, we examined use of WorldPop (Tatem 2017) estimates for 2016, which are also available on a 100 m × 100 m resolution. Although provided at a high resolution, we found the WorldPop estimates lacked the spatial heterogeneity available in other population data sets. Although population estimates are still a source of uncertainty in our assessment, we believe using a data set specific to the United States that incorporates both census and satellite data reduced part of this uncertainty. Among our pollutant concentration data sets, the Street View data set included only measurements that were taken during the daytime and on weekdays and may not, therefore, have fully captured long-term annual averages. The LUR data set incorporates *in situ* data, although concentrations are ultimately estimations of the sum of all oxidized atmospheric odd-nitrogen species (NO_y) estimations and not observations of actual NO_2 concentrations (Dickerson et al. 2019). Future work can make use of more spatially refined estimates of $PM_{2.5}$ (Di et al. 2019). In addition, NO_2 satellite-derived models have now been developed (Di et al. 2020) that can be compared with results from LUR models.

In addition, we assumed a causal relationship between NO_2 and all-cause mortality, although the putative agent(s) in the traffic-related pollution mixture are unknown, adding to uncertainty in our estimates. Epidemiological studies often use NO_2 as a marker of traffic-related air pollution because it is easily measured and for consistency in characterizing spatial patterns in traffic-related air pollution (Beckerman et al. 2008; Levy et al. 2014). However, none of the studies in the meta-analysis we used to derive RRs for NO_2 and all-cause and CVD mortality adjusted for traffic-related particles or other chemicals, including BC and $PM_{2.5}$, in the traffic pollution mixture (Atkinson and Butland 2018). It therefore remains unclear whether NO_2 itself is associated with mortality or whether NO_2 serves as a proxy for other elements of the traffic-related air pollution mixture. Following COMEAP recommendations, the NO_2 mortality impacts should be interpreted as a metric of the overall mortality burden due to mixture of near field traffic-related air pollution.

Another challenge with hyperlocal air pollution health impact assessment that requires further exploration was capturing pollution exposure accurately for population movement. We believe this limitation was mitigated for two reasons: *a*) air pollution disproportionately affects the very young and very old, who tend to stay closer to home throughout the day (Chambers et al. 2017; Spalt et al. 2016); and *b*) most air pollution epidemiological studies use residential address as the method of assigning exposure, thus accounting for population movement would be inconsistent with the epidemiological studies from which we drew concentration–response relationships. In addition, using only residential address in exposure assessment within epidemiological studies has been found to underestimate health effects of $PM_{2.5}$ by about 10% (Nyhan et al. 2019). Similarly, without information available on the time-varying activity patterns of our population, we were unable to account for time–activity data in our risk assessment; however, exposure misclassification likely contributed less than other variables (e.g., RRs) to uncertainty in our health impact results. Our results indicate population movement out of highly polluted areas may substantially reduce population pollutant-attributable health burden. However, this points to the need for more epidemiological analysis using exposure assessment techniques beyond central site monitors, as well as techniques that account for people's movements rather than assigning exposure at the residential address. This factor should be explored in greater detail to understand how population movement affects actual exposure levels and estimated health impact assessment results. A related limitation is that the high-resolution concentration data sets we used did not match the exposure assessment techniques used in the epidemiological studies from which we derived our CRF, which most frequently used stationary monitors and, increasingly, LUR and satellite-based models, which may be more coarsely resolved than the data sets we used here. Thus, the CRFs we applied may be inconsistent with the exposure estimates we used.

Some recommended best practices in conducting air pollution health impact assessments in cities globally can be derived from the insights from this work. First, we found that applying fine-scale mobile monitoring or satellite LUR-derived air pollution data in health impact assessment reveals large and unequal distributions of the air pollution burden in cities. This indicates that spatial distribution of air pollution impacts could be routinely assessed in city air quality health impact assessments. Second, the distribution of air pollution and its risks and burdens did not follow the same patterns owing to large underlying spatial health disparities (reflected in baseline disease rates) and population distribution. Although most of the research in this area has focused on producing increasingly fine resolution estimates of air

pollutant concentrations, similar emphasis has not been given to estimating or measuring spatial patterns of disease. Ignoring health disparities results in underestimating air pollution impacts in areas already burdened by poor health and masks the disproportionate impact faced by disadvantaged communities within cities. This has important environmental justice implications, and local disease rates should be incorporated as a best practice into city air pollution health impact assessments.

Conclusions

We found that air pollution health risks vary considerably within cities and that information on the spatial distribution of pollutant concentrations alone is insufficient to identify areas of elevated risk and burden of disease attributable to air pollution. We anticipate that these findings will apply to other health impact assessments conducted on the local scale given that spatial heterogeneity in disease rates is not unique to the Bay Area. Using pollutant concentrations from predictive models and mobile monitoring measurements identify similar spatial patterns of disease because disparities in baseline disease rates drive a substantial portion of heterogeneity in air pollution-attributable health risks. For areas with limited resources or where intensive mobile monitoring is not feasible, LUR- and satellite-derived models may be sufficient for identifying intra-urban areas of elevated risk, but additional research is needed to determine whether these findings hold in other areas. In addition, LUR- and satellite-derived models typically do not account for the mixture of vehicle types and traffic volume and, therefore, may be improved with the information about roadway concentrations captured in mobile monitoring data sets. Future work may seek to integrate multiple sources of pollutant concentration information to leverage the advantages of each. It is also important to expand reporting of disease rates at subcity scales.

Acknowledgments

This study was supported by the National Aeronautics and Space Administration grant 80NSSC19K0193 and a gift to Environmental Defense Fund from Signe Ostby and Scott Cook, Valhalla Foundation. The authors thank Aclima Inc., Google Earth Outreach, and Google Street View for providing and operating the mobile monitoring platform and sharing air quality measurements. Code for the health impact assessment calculations is available at https://github.com/vtinney/EDF-GWU-Hyperlocal-HIA/.

References

Achakulwisut P, Brauer M, Hystad P, Anenberg SC. 2019. Global, national, and urban burdens of paediatric asthma incidence attributable to ambient NO_2 pollution: estimates from global datasets. Lancet Planet Health 3(4):e166–e178, PMID: 30981709, https://doi.org/10.1016/S2542-5196(19)30046-4.

Aclima, Environmental Defense Fund, Google Earth Outreach, University of Texas at Austin. 2019. Street View Air Quality Dataset, Bay Area Mobile Analysis. https://aqdatacommons.org/explore [accessed 8 June 2020].

Alexeeff SE, Roy A, Shan J, Liu X, Messier K, Apte JS, et al. 2018. High-resolution mapping of traffic related air pollution with Google Street View cars and incidence of cardiovascular events within neighborhoods in Oakland, CA. Environ Health 17(1):38, PMID: 29759065, https://doi.org/10.1186/s12940-018-0382-1.

Alotaibi R, Bechle M, Marshall JD, Ramani T, Zietsman J, Nieuwenhuijsen MJ, et al. 2019. Traffic related air pollution and the burden of childhood asthma in the contiguous United States in 2000 and 2010. Environ Int 127:858–867, PMID: 30954275, https://doi.org/10.1016/j.envint.2019.03.041.

Anenberg SC, Achakulwisut P, Brauer M, Moran D, Apte JS, Henze DK. 2019. Particulate matter-attributable mortality and relationships with carbon dioxide in 250 urban areas worldwide. Sci Rep 9(1):11552, PMID: 31399636, https://doi.org/10.1038/s41598-019-48057-9.

Anenberg SC, Miller J, Minjares R, Du L, Henze DK, Lacey F, et al. 2017. Impacts and mitigation of excess diesel-related NO_x emissions in 11 major vehicle markets. Nature 545(7655):467–471, PMID: 28505629, https://doi.org/10.1038/nature22086.

Anenberg SC, Schwartz J, Shindell D, Amann M, Faluvegi G, Klimont Z, et al. 2012. Global air quality and health co-benefits of mitigating near-term climate change through methane and black carbon emission controls. Environ Health Perspect 120(6):831–839, PMID: 22418651, https://doi.org/10.1289/ehp.1104301.

Apte JS, Messier KP, Gani S, Brauer M, Kirchstetter TW, Lunden MM, et al. 2017. High-resolution air pollution mapping with Google Street View cars: exploiting big data. Environ Sci Technol 51(12):6999–7008, PMID: 28578585, https://doi.org/10.1021/acs.est.7b00891.

Atkinson RW, Butland BK. 2018. Working paper 1: systematic review and meta-analysis of cohort studies of NO_2 and all-cause mortality. Working paper for COMEAP Report "Associations of long-term average concentrations of nitrogen dioxide with mortality." July 2018. https://assets.publishing.service.gov.uk/government/uploads/system/uploads/attachment_data/file/734802/COMEAP_NO2_Working_Paper_1.pdf [accessed 8 June 2020].

Atkinson RW, Butland BK, Anderson HR, Maynard RL. 2018. Long-term concentrations of nitrogen dioxide and mortality: a meta-analysis of cohort studies. Epidemiology 29(4):460–472, PMID: 29746370, https://doi.org/10.1097/EDE.0000000000000847.

BAAQMD (Bay Area Air Quality Management District). 2017. Spare the Air—Cool the Climate: a Blueprint for Clean Air and Climate Protection in the Bay Area. Final 2017 Clean Air Plan. San Francisco, CA: Bay Area Air Quality Management District. https://www.baaqmd.gov/~/media/files/ab617-community-health/west-oakland/100219-files/final-plan-vol-1-100219-pdf.pdf?la=en [accessed 16 March 2021].

BAAQMD, West Oakland Environmental Indicators Project. 2019. Owning Our Air: the West Oakland Community Action Plan—Volume 1: the Plan. http://www.baaqmd.gov/~/media/files/ab617-community-health/west-oakland/100219-files/final-plan-vol-1-100219-pdf.pdf?la=en [accessed 8 June 2020].

Bechle MJ, Millet DB, Marshall JD. 2015. National spatiotemporal exposure surface for NO_2: monthly scaling of a satellite-derived land-use regression, 2000–2010. Environ Sci Technol 49(20):12297–12305, PMID: 26397123, https://doi.org/10.1021/acs.est.5b02882.

Beckerman B, Jerrett M, Brook JR, Verma DK, Arain MA, Finkelstein MM. 2008. Correlation of nitrogen dioxide with other traffic pollutants near a major expressway. Atmos Environ 42(2):275–290, https://doi.org/10.1016/j.atmosenv.2007.09.042.

Bhaduri B, Bright E, Coleman P, Urban ML. 2007. LandScan USA: a high-resolution geospatial and temporal modeling approach for population distribution and dynamics. GeoJournal 69(1–2):103–117, https://doi.org/10.1007/s10708-007-9105-9.

Bravo MA, Ebisu K, Dominici F, Wang Y, Peng RD, Bell ML. 2017. Airborne fine particles and risk of hospital admissions for understudied populations: effects by urbanicity and short-term cumulative exposures in 708 U.S. counties. Environ Health Perspect 125(4):594–601, PMID: 27649448, https://doi.org/10.1289/EHP257.

Brillinger DR. 1986. The natural variability of vital rates and associated statistics. Biometrics 42(4):693–734, PMID: 3814721, https://doi.org/10.2307/2530689.

Brønnum-Hansen H, Bender AM, Andersen ZJ, Sørensen J, Bønløkke JH, Boshuizen H, et al. 2018. Assessment of impact of traffic-related air pollution on morbidity and mortality in Copenhagen Municipality and the health gain of reduced exposure. Environ Int 121(pt 1):973–980, PMID: 30408890, https://doi.org/10.1016/j.envint.2018.09.050.

Caiazzo F, Ashok A, Waitz IA, Yim SHL, Barrett SRH. 2013. Air pollution and early deaths in the United States. Part I: quantifying the impact of major sectors in 2005. Atmos Environ 79:198–208, https://doi.org/10.1016/j.atmosenv.2013.05.081.

Cal AB 617 (California Assembly Bill 627). 2017. https://leginfo.legislature.ca.gov/faces/billNavClient.xhtml?bill_id=201720180AB617 [accessed 9 March 2021].

CDC (Centers for Disease Control). 2018. CDC WONDER. https://wonder.cdc.gov/ [accessed 8 June 2020].

CDPH (California Department of Health). 2017. Asthma ED Visit Rates (LGHC Indicator). https://data.chhs.ca.gov/dataset/asthma-ed-visit-rates-lghc-indicator-07 [accessed 8 June 2020].

CDPH. 2019. Asthma ED visit rates by ZIP code. https://data.ca.gov/dataset/asthma-emergency-department-visit-rates/resource/d6574ae2-983b-4bd7-a0c6-0572389a9de8 [accessed 8 June 2020].

Chambers T, Pearson AL, Kawachi I, Rzotkiewicz Z, Stanley J, Smith M, et al. 2017. Kids in space: measuring children's residential neighborhoods and other destinations using activity space GPS and wearable camera data. Soc Sci Med 193:41–50, PMID: 28992540, https://doi.org/10.1016/j.socscimed.2017.09.046.

Chowdhury S, Dey S. 2016. Cause-specific premature death from ambient $PM_{2.5}$ exposure in India: estimate adjusted for baseline mortality. Environ Int 91:283–290, PMID: 27063285, https://doi.org/10.1016/j.envint.2016.03.004.

CIESEN (Center for International Earth Science Information Network). 2019. Gridded Population of the World (GPW), v4. Palisades, NY: NASA Socioeconomic Data and Applications Center. http://sedac.ciesin.columbia.edu/data/collection/gpw-v4 [accessed 8 June 2020].

Cohen AJ, Brauer M, Burnett R, Anderson HR, Frostad J, Estep K, et al. 2017. Estimates and 25-year trends of the global burden of disease attributable to

ambient air pollution: an analysis of data from the Global Burden of Diseases Study 2015. Lancet 389(10082):1907–1918, PMID: 28408086, https://doi.org/10.1016/S0140-6736(17)30505-6.

COMEAP (Committee on the Medical Effects of Air Pollutants). 2018. *Associations of Long-Term Average Concentrations of Nitrogen Dioxide with Mortality*. https://assets.publishing.service.gov.uk/government/uploads/system/uploads/attachment_data/file/734799/COMEAP_NO2_Report.pdf [accessed 8 June 2020].

Crouse DL, Peters PA, van Donkelaar A, Goldberg MS, Villeneuve PJ, Brion O, et al. 2012. Risk of nonaccidental and cardiovascular mortality in relation to long-term exposure to low concentrations of fine particulate matter: a Canadian national-level cohort study. Environ Health Perspect 120(5):708–714, PMID: 22313724, https://doi.org/10.1289/ehp.1104049.

Crouse DL, Peters PA, Villeneuve PJ, Proux MO, Shin HH, Goldberg MS, et al. 2015. Within- and between-city contrasts in nitrogen dioxide and mortality in 10 Canadian cities; a subset of the Canadian CanCHEC (Census Health and Environment Cohort). J Expo Sci Environ Epidemiol 25(5):482–489, PMID: 25605445, https://doi.org/10.1038/jes.2014.89.

Di Q, Amini H, Shi L, Kloog I, Silvern R, Kelly J, et al. 2019. An ensemble-based model of $PM_{2.5}$ concentration across the contiguous United States with high spatiotemporal resolution. Environ Int 130:104909, PMID: 31272018, https://doi.org/10.1016/j.envint.2019.104909.

Di Q, Amini H, Shi L, Kloog I, Silvern R, Kelly J, et al. 2020. Assessing NO_2 concentration and model uncertainty with high spatiotemporal resolution across the contiguous United States using ensemble model averaging. Environ Sci Technol 54(3):1372–1384, PMID: 31851499, https://doi.org/10.1021/acs.est.9b03358.

Di Q, Kloog I, Koutrakis P, Lyapustin A, Wang Y, Schwartz J. 2016. Assessing $PM_{2.5}$ exposures with high spatiotemporal resolution across the continental United States. Environ Sci Technol 50(9):4712–4721, PMID: 27023334, https://doi.org/10.1021/acs.est.5b06121.

Di Q, Wang Y, Zanobetti A, Wang Y, Koutrakis P, Choirat C, et al. 2017. Air pollution and mortality in the Medicare population. N Engl J Med 376(26):2513–2522, PMID: 28657878, https://doi.org/10.1056/NEJMoa1702747.

Diao M, Holloway T, Choi S, O'Neill SM, Al-Hamdan MZ, Van Donkelaar A, et al. 2019. Methods, availability, and applications of $PM_{2.5}$ exposure estimates derived from ground measurements, satellite, and atmospheric models. J Air Waste Manag Assoc 69(12):1391–1414, PMID: 31526242, https://doi.org/10.1080/10962247.2019.1668498.

Dickerson RR, Anderson DC, Ren X. 2019. On the use of data from commercial NOx analyzers for air pollution studies. Atmos Environ 214:116873, https://doi.org/10.1016/j.atmosenv.2019.116873.

Dominici F, Peng RD, Barr CD, Bell ML. 2010. Protecting human health from air pollution: shifting from a single-pollutant to a multi-pollutant approach. Epidemiology (Cambridge, Mass.) 21(2):187–194, PMID: 20160561, https://doi.org/10.1097/EDE.0b013e3181cc86e8.

Duncan BN, Lamsal LN, Thompson AM, Yoshida Y, Lu Z, Streets DG, et al. 2016. A space-based, high-resolution view of notable changes in urban NO_x pollution around the world (2005–2014). J Geophys Res Atmos 121(2):976–996, https://doi.org/10.1002/2015JD024121.

Eayres D, Williams ES. 2004. Evaluation of methodologies for small area life expectancy estimation. J Epidemiol Community Health 58(3):243–249, PMID: 14966240, https://doi.org/10.1136/jech.2003.009654.

Environmental Justice Task Force. 2017. *Oakland Initiative Report*. Sacramento, CA: California Environmental Protection Agency. https://calepa.ca.gov/wp-content/uploads/sites/6/2018/03/OAKEJ_initiative_FINALweb.pdf [accessed 8 June 2020].

Eum KD, Kazemiparkouhi F, Wang B, Manjourides J, Pun V, Pavlu V, et al. 2019. Long-term NO_2 exposures and cause-specific mortality in American older adults. Environ Int 124:10–15, PMID: 30639903, https://doi.org/10.1016/j.envint.2018.12.060.

Fann N, Kim SY, Olives C, Sheppard L. 2017. Estimated changes in life expectancy and adult mortality resulting from declining $PM_{2.5}$ exposures in the contiguous United States: 1980–2010. Environ Health Perspect 125(9):097003, PMID: 28934094, https://doi.org/10.1289/EHP507.

Fann N, Lamson AD, Anenberg SC, Wesson K, Risley D, Hubbell BJ. 2012. Estimating the national public health burden associated with exposure to ambient $PM_{2.5}$ and ozone. Risk Anal 32(1):81–95, PMID: 21627672, https://doi.org/10.1111/j.1539-6924.2011.01630.x.

Fenech S, Doherty RM, Heaviside C, Vardoulakis S, Macintyre HL, O'Connor FM. 2018. The influence of model spatial resolution on simulated ozone and fine particulate matter for Europe: implications for health impact assessments. Atmos Chem Phys 18(8):5765–5784, https://doi.org/10.5194/acp-18-5765-2018.

GBD 2017 Risk Factor Collaborators. 2018. Global, regional, and national comparative risk assessment of 84 behavioural, environmental and occupational, and metabolic risks or clusters of risks for 195 countries and territories, 1990–2017: a systematic analysis for the Global Burden of Disease Study 2017. Lancet 392(10159):1923–1994, PMID: 30496105, https://doi.org/10.1016/S0140-6736(18)32225-6.

Grant M, Brown C, Caiaffa WT, Capon A, Corburn J, Coutts C, et al. 2017. Cities and health: an evolving global conversation. Cities Health 1(1):1–9, https://doi.org/10.1080/23748834.2017.1316025.

Hubbell B, Fann N, Levy JI. 2009. Methodological considerations in developing local-scale health impact assessments: balancing national, regional, and local data. Air Qual Atmos Health 2(2):99–110, https://doi.org/10.1007/s11869-009-0037-z.

Hystad P, Setton E, Cervantes A, Poplawski K, Deschenes S, Brauer M, et al. 2011. Creating national air pollution models for population exposure assessment in Canada. Environ Health Perspect 119(8):1123–1129, PMID: 21454147, https://doi.org/10.1289/ehp.1002976.

Janssen NAH, Hoek G, Simic-Lawson M, Fischer P, van Bree L, ten Brink H, et al. 2011. Black carbon as an additional indicator of the adverse health effects of airborne particles compared with PM_{10} and $PM_{2.5}$. Environ Health Perspect 119(12):1691–1699, PMID: 21810552, https://doi.org/10.1289/ehp.1003369.

Kheirbek I, Wheeler K, Walters S, Kass D, Matte T. 2013. $PM_{2.5}$ and ozone health impacts and disparities in New York City: sensitivity to spatial and temporal resolution. Air Qual Atmos Health 6(2):473–486, PMID: 23710262, https://doi.org/10.1007/s11869-012-0185-4.

Khreis H, Kelly C, Tate J, Parslow R, Lucas K, Nieuwenhuijsen M. 2017. Exposure to traffic-related air pollution and risk of development of childhood asthma: a systematic review and meta-analysis. Environ Int 100:1–31, PMID: 27881237, https://doi.org/10.1016/j.envint.2016.11.012.

Kihal-Talantikite W, Legendre P, Le Nouveau P, Deguen S. 2018. Premature adult death and equity impact of a reduction of NO_2, PM_{10}, and $PM_{2.5}$ levels in Paris—a health impact assessment study conducted at the census block level. Int J Environ Res Public Health 16(1):38, PMID: 30586915, https://doi.org/10.3390/ijerph16010038.

Kioumourtzoglou MA, Austin E, Koutrakis P, Dominici F, Schwartz J, Zanobetti A. 2015. $PM_{2.5}$ and survival among older adults: effect modification by particulate composition. Epidemiology 26(3):321–327, PMID: 25738903, https://doi.org/10.1097/EDE.0000000000000269.

Korhonen A, Lehtomäki H, Rumrich I, Karvosenoja N, Paunu VV, Kupiainen K, et al. 2019. Influence of spatial resolution on population $PM_{2.5}$ exposure and health impacts. Air Qual Atmos Health 12(6):705–718, https://doi.org/10.1007/s11869-019-00690-z.

Krewski D, Jerrett M, Burnett RT, Ma R, Hughes E, Shi Y, et al. 2009. Extended follow-up and spatial analysis of the American Cancer Society study linking particulate air pollution and mortality. Res Rep Health Eff Inst 140:5–114, PMID: 19627030.

Krzyzanowski M, Apte JS, Bonjour SP, Brauer M, Cohen AJ, Prüss-Ustun AM. 2014. Air pollution in the mega-cities. Curr Envir Health Rep 1(3):185–191, https://doi.org/10.1007/s40572-014-0019-7.

Larkin A, Geddes JA, Martin RV, Xiao Q, Liu Y, Marshall JD, et al. 2017. Global land use regression model for nitrogen dioxide air pollution. Environ Sci Technol 51(12):6957–6964, PMID: 28520422, https://doi.org/10.1021/acs.est.7b01148.

Levy I, Mihele C, Lu G, Narayan J, Brook JR. 2014. Evaluating multipollutant exposure and urban air quality: pollutant interrelationships, neighborhood variability, and nitrogen dioxide as a proxy pollutant. Environ Health Perspect 122(1):65–72, PMID: 24225648, https://doi.org/10.1289/ehp.1306518.

Li Y, Henze DK, Jack D, Kinney PL. 2016. The influence of air quality model resolution on health impact assessment for fine particulate matter and its components. Air Qual Atmos Health 9(1):51–68, PMID: 28659994, https://doi.org/10.1007/s11869-015-0321-z.

Lim H, Kwon HJ, Lim JA, Choi JH, Ha M, Hwang SS, et al. 2016. Short-term effect of fine particulate matter on children's hospital admissions and emergency department visits for asthma: a systematic review and meta-analysis. J Prev Med Public Health 49(4):205–219, PMID: 27499163, https://doi.org/10.3961/jpmph.16.037.

Marlier ME, Jina AS, Kinney PL, DeFries RS. 2016. Extreme air pollution in global megacities. Curr Clim Change Rep 2(1):15–27, https://doi.org/10.1007/s40641-016-0032-z.

Martenies SE, Milando CW, Batterman SA. 2018. Air pollutant strategies to reduce adverse health impacts and health inequalities: a quantitative assessment for Detroit, Michigan. Air Qual Atmos Health 11(4):409–422, PMID: 30220936, https://doi.org/10.1007/s11869-017-0543-3.

Messier KP, Chambliss SE, Gani S, Alvarez R, Brauer M, Choi JJ, et al. 2018. Mapping air pollution with Google Street View cars: efficient approaches with mobile monitoring and land use regression. Environ Sci Technol 52(21):12563–12572, PMID: 30354135, https://doi.org/10.1021/acs.est.8b03395.

Milet M, Lutzker L, Flattery J. 2013. *Asthma in California: a Surveillance Report*. Richmond, CA: California Department of Public Health, Environmental Health Investigations Branch. https://www.cdph.ca.gov/Programs/CCDPHP/DEODC/EHIB/CPE/CDPH%20Document%20Library/Asthma_in_California_2013.pdf [accessed 8 June 2020].

Mueller N, Rojas-Rueda D, Basagaña X, Cirach M, Cole-Hunter T, Dadvand P, et al. 2017. Urban and transport planning related exposures and mortality: a health impact assessment for cities. Environ Health Perspect 125(1):89–96, PMID: 27346385, https://doi.org/10.1289/EHP220.

Mueller N, Rojas-Rueda D, Khreis H, Cirach M, Andrés D, Ballester J, et al. 2020. Changing the urban design of cities for health: the superblock model. Environ Int 134:105132, PMID: 31515043, https://doi.org/10.1016/j.envint.2019.105132.

Mueller N, Rojas-Rueda D, Khreis H, Cirach M, Milà C, Espinosa A, et al. 2018. Socioeconomic inequalities in urban and transport planning related exposures and mortality: a health impact assessment study for Bradford, UK. Environ Int 121(pt 1):931–941, PMID: 30347375, https://doi.org/10.1016/j.envint.2018.10.017.

Nethery RC, Dominici F. 2019. Estimating pollution-attributable mortality at the regional and global scales: challenges in uncertainty estimation and causal inference. Eur Heart J 40(20):1597–1599, PMID: 31004133, https://doi.org/10.1093/eurheartj/ehz200.

Nyhan MM, Kloog I, Britter R, Ratti C, Koutrakis P. 2019. Quantifying population exposure to air pollution using individual mobility patterns inferred from mobile phone data. J Expo Sci Environ Epidemiol 29(2):238–247, PMID: 29700403, https://doi.org/10.1038/s41370-018-0038-9.

Oak Ridge National Laboratories. 2020. LandScan USA. https://geoplatform.maps.arcgis.com/home/item.html?id=e431a6410145450aa56606568345765b [accessed 8 June 2020].

Ord J, Getis A. 1995. Local spatial autocorrelation statistics: distributional issues and an application. Geograph Anal 27(4):286–306, https://doi.org/10.1111/j.1538-4632.1995.tb00912.x.

Orellano P, Quaranta N, Reynoso J, Balbi B, Vasquez J. 2017. Effect of outdoor air pollution on asthma exacerbations in children and adults: systematic review and multilevel meta-analysis. PLoS One 12(3):e0174050, PMID: 28319180, https://doi.org/10.1371/journal.pone.0174050.

Paolella DA, Tessum CW, Adams PJ, Apte JS, Chambliss S, Hill J, et al. 2018. Effect of model spatial resolution on estimates of fine particulate matter exposure and exposure disparities in the United States. Environ Sci Technol Lett 5(7):436–441, https://doi.org/10.1021/acs.estlett.8b00279.

Peng RD, Bell ML, Geyh AS, McDermott A, Zeger SL, Samet JM, et al. 2009. Emergency admissions for cardiovascular and respiratory diseases and the chemical composition of fine particle air pollution. Environ Health Perspect 117(6):957–963, PMID: 19590690, https://doi.org/10.1289/ehp.0800185.

Pickle LW, White AA. 1995. Effects of the choice of age-adjustment method on maps of death rates. Stat Med 14(5–7):615–627, PMID: 7792452, https://doi.org/10.1002/sim.4780140519.

Pierangeli I, Nieuwenhuijsen MJ, Cirach M, Rojas-Rueda D. 2020. Health equity and burden of childhood asthma—related to air pollution in Barcelona. Environ Res 186:109067, PMID: 32037015, https://doi.org/10.1016/j.envres.2019.109067.

Punger EM, West JJ. 2013. The effect of grid resolution on estimates of the burden of ozone and fine particulate matter on premature mortality in the United States. Air Quality Atmos Health 6(3):563–573, PMID: 24348882, https://doi.org/10.1007/s11869-013-0197-8.

Sacks JD, Lloyd JM, Zhu Y, Anderton J, Jang CJ, Hubbell B, et al. 2018. The Environmental Benefits Mapping and Analysis Program – Community Edition (BenMAP–CE): a tool to estimate the health and economic benefits of reducing air pollution. Environ Model Softw 104:118–129, PMID: 29962895, https://doi.org/10.1016/j.envsoft.2018.02.009.

Shaddick G, Thomas ML, Amini H, Broday D, Cohen A, Frostad J, et al. 2018. Data integration for the assessment of population exposure to ambient air pollution for global burden of disease assessment. Environ Sci Technol 52(16):9069–9078, PMID: 29957991, https://doi.org/10.1021/acs.est.8b02864.

Spalt EW, Curl CL, Allen RW, Cohen M, Adar SD, Stukovsky KH, et al. 2016. Time–location patterns of a diverse population of older adults: the Multi-Ethnic Study of Atherosclerosis and Air Pollution (MESA AIR). J Expo Sci Environ Epidemiol 26(4):349–355, PMID: 25921083, https://doi.org/10.1038/jes.2015.29.

Stafoggia M, Breitner S, Hampel R, Basagaña X. 2017. Statistical approaches to address multi-pollutant mixtures and multiple exposures: the state of the science. Curr Environ Health Rep 4(4):481–490, PMID: 28988291, https://doi.org/10.1007/s40572-017-0162-z.

Stephens C. 2018. Healthy cities or unhealthy islands? The health and social implications of urban inequality. Urbanisation 3(2):108–130, https://doi.org/10.1177/2455747118805840.

Tatem AJ. 2017. WorldPop, open data for spatial demography. Sci Data 4:170004, PMID: 28140397, https://doi.org/10.1038/sdata.2017.4.

Thompson TM, Saari RK, Selin NE. 2014. Air quality resolution for health impact assessment: influence of regional characteristics. Atmospheric Chemistry and Physics 14(2):969–978, https://doi.org/10.5194/acp-14-969-2014.

Thurston GD, Burnett RT, Turner MC, Shi Y, Krewski D, Lall R, et al. 2016. Ischemic heart disease mortality and long-term exposure to source-related components of U.S. fine particle air pollution. Environ Health Perspect 124(6):785–794, PMID: 26629599, https://doi.org/10.1289/ehp.1509777.

Turner MC, Jerrett M, Pope CA III, Krewski D, Gapstur SM, Diver WR, et al. 2016. Long-term ozone exposure and mortality in a large prospective study. Am J Respir Crit Care Med 193(10):1134–1142, PMID: 26680605, https://doi.org/10.1164/rccm.201508-1633OC.

U.S. Census Bureau. 2018. Urban areas facts. https://www.census.gov/programs-surveys/geography/guidance/geo-areas/urban-rural/ua-facts.html [accessed 6 February 2021].

U.S. EPA (U.S. Environmental Protection Agency). 2016. *Integrated Science Assessment (ISA) for Oxides of Nitrogen—Health Criteria (Final Report)*. Washington, DC: U.S. EPA. EPA/600/R-15-068. https://ofmpub.epa.gov/eims/eimscomm.getfile?p_download_id=526855 [accessed 8 June 2020].

U.S. EPA. 2019. *Integrated Science Assessment (ISA) for Particulate Matter (Final Report)*. Washington, DC: U.S. EPA. EPA/600/R-19/188. https://ofmpub.epa.gov/eims/eimscomm.getfile?p_download_id=539935 [accessed 8 June 2020].

United Nations. 2019. *World Urbanization Prospects: the 2018 Revision*. ST/ESA/SER.A/420. New York, NY: United Nations, Department of Economic and Social Affairs, Population Division. https://population.un.org/wup/Publications/Files/WUP2018-Report.pdf [accessed 6 February 2021].

van Donkelaar A, Martin RV, Brauer M, Hsu NC, Kahn RA, Levy RC, et al. 2016. Global estimates of fine particulate matter using a combined geophysical-statistical method with information from satellites, models, and monitors. Environ Sci Technol 50(7):3762–3772, PMID: 26953851, https://doi.org/10.1021/acs.est.5b05833.

van Donkelaar A, Martin RV, Li C, Burnett RT. 2019. Regional estimates of chemical composition of fine particulate matter using a combined geoscience-statistical method with information from satellites, models, and monitors. Environ Sci Technol 53(5):2595–2611, PMID: 30698001, https://doi.org/10.1021/acs.est.8b06392.

Vodonos A, Awad YA, Schwartz J. 2018. The concentration-response between long-term $PM_{2.5}$ exposure and mortality; a meta-regression approach. Environ Res 166:677–689, PMID: 30077140, https://doi.org/10.1016/j.envres.2018.06.021.

WHO (World Health Organization). 2016. *International Statistical Classification of Diseases and Related Health Problems, 10th Revision*. http://apps.who.int/classifications/icd10/browse/2016/en [accessed 9 March 2021].

Zhang Y, West JJ, Mathur R, Xing J, Hogrefe C, Roselle SJ, et al. 2018. Long-term trends in the ambient $PM_{2.5}$- and O_3-related mortality burdens in the United States under emission reductions from 1990 to 2010. Atmos Chem Phys 18(20):15003–15016, PMID: 30930942, https://doi.org/10.5194/acp-18-15003-2018.

Zheng XY, Ding H, Jiang LN, Chen SW, Zheng JP, Qiu M, et al. 2015. Association between air pollutants and asthma emergency room visits and hospital admissions in time series studies: a systematic review and meta-analysis. PLoS One 10(9):e0138146, PMID: 26382947, https://doi.org/10.1371/journal.pone.0138146.